# Optimization of IIR Digital Filters Using Differential Evolution: A Comparative Analysis of FDDE and AMECoDEs Algorithms

Wildor Ferrel Serruto
Departamento Académico de Ingeniería Electrónica, Universidad Nacional de San Agustín de Arequipa, Arequipa, Perú

***Abstract*—Infinite impulse response (IIR) digital filters are fundamental components in various digital signal processing applications, particularly those requiring optimized use of computational resources, such as memory and processing power. This study presents the design of classical IIR filters, including low-pass, high-pass, band-pass, and band-stop configurations, as well as multiple-passband filters featuring dual and triple passbands. Two differential evolution algorithms are utilized: FDDE (Differential Evolution Algorithm with Fitness and Diversity Ranking-Based Mutation Operator) and AMECoDEs (Adaptive Multiple-Elites-Guided Composite Differential Evolution Algorithm with a Shift Mechanism). To date, no study has investigated the application of the FDDE algorithm to IIR digital filter design, whereas the AMECoDEs algorithm has seen limited application in this context. Consequently, this work investigates the design of IIR filters using these algorithms and assesses their performance based on the mean squared error (MSE). Comparative analysis reveals that, for classical filters, the FDDE algorithm yields a slightly lower MSE in the magnitude response compared to the AMECoDEs algorithm. Conversely, for multiple-passband filters, the AMECoDEs algorithm outperforms FDDE by achieving a lower MSE. In the proposed model, IIR filters are implemented using a cascade structure of second-order sections (SOS), with their fitness function evaluated based on the MSE, computed using a constant weight function within each frequency band. Additionally, the magnitude response characteristics of the designed filters are compared with those of classical and dual-passband filters designed with the AMECoDEs algorithm in recent studies. The results indicate that the filters designed in this study show significant improvements across most evaluated metrics, particularly in terms of improved stopband attenuation. One of the key contributions of this work is the novel application of differential evolution algorithms to the design of triple-passband IIR filters, demonstrating their effectiveness through successful validation on a development board.**

***Keywords*—IIR digital filter; differential evolution; FDDE algorithm; AMECoDEs algorithm; triple-passband IIR filter**

## I. Introduction

Digital filters are integral components of many digital signal processing systems. Because of their ability to manipulate signals flexibly and precisely, digital filters are used in various areas such as audio signal processing [1], [2], digital communications [3], automation and control [4], [5], and biomedical signal processing [6], [7].

The mathematical tools used in the analysis, design, and characterization of digital filters include the transfer function, frequency response, and impulse response, which provide insight into their behavior in both the frequency and time domains. The transfer function of a digital filter takes the form given in Eq. (1):

$$H(z) = \frac{b_0 + b_1 z^{-1} + \ldots + b_P z^{-P}}{1 + a_1 z^{-1} + \ldots + a_Q z^{-Q}} \tag{1}$$

The order of a digital filter is the maximum of the degree of the numerator polynomial and the degree of the denominator polynomial of the transfer function. In Eq. (1), the filter's order is $\max(P, Q)$. Based on the length of the impulse response, digital filters are classified into finite impulse response (FIR) filters and infinite impulse response (IIR) filters. When all the denominator coefficients satisfy $a_1 = a_2 = \ldots = a_Q = 0$ in Eq. (1), the filter is classified as FIR; otherwise, it is classified as IIR.

If an IIR filter is designed while ensuring its stability and an FIR filter is designed with the same specifications—such as identical frequency bands, maximum attenuation in the passbands, and minimum attenuation in the stopbands—the IIR filter will have a lower order compared to the FIR filter. This implies that IIR filters are more computationally efficient in terms of processing time. Due to this advantage, IIR digital filters are widely applied across various domains, including digital equalizer design [8], noise removal from electrocardiogram (ECG) signals [9], [10], [11], signal filtering for perception system sensors in autonomous vehicles [12], and hotspot identification in the COVID-19 disease protein sequence [13], among others. It is important to note that attenuation in decibels (dB) is equal to gain in decibels with the sign reversed.

The design of digital filters is a critical task in various applications, as the quality of the processed signal largely depends on the effectiveness of the applied filter. Methods for designing IIR filters can be classified into two main categories: conventional methods and optimization-based methods [14]. Conventional methods have been extensively studied and rely on mathematical equations and analytical techniques to achieve the desired filter response, typically utilizing analog filter prototypes such as Butterworth, Chebyshev, and elliptic filters. In contrast, optimization-based methods employ algorithms and numerical techniques to determine the filter coefficients that minimize a predefined error criterion, such as the mean squared error. These methods offer greater flexibility in addressing complex design specifications, allowing for the synthesis of

filters that simultaneously satisfy multiple constraints. Consequently, optimization-based approaches have received growing attention in recent literature.

### A. Research Contribution

The key contributions of this study are as follows:

- First-time utilization of the FDDE algorithm for the design of IIR digital filters, expanding its applicability within the field of digital signal processing.
- Comparative analysis of the FDDE and AMECoDEs algorithms in the design of classical and multi-passband IIR filters, highlighting their respective advantages.
- Performance assessment of the designed filters based on mean squared error (MSE), computed using a constant weight function within each frequency band, in contrast to previous studies where a linear weight function was employed.
- Novel application of differential evolution algorithms to the design of triple-passband IIR filters, demonstrating their effectiveness through successful validation on a development board.

The remainder of this article is organized as follows: Section II reviews prior works. Section III introduces the Differential Evolution algorithm. Section IV defines the problem addressed in this study. Section V provides a detailed explanation of the FDDE algorithm for IIR digital filter design. Section VI describes the proposed methodology. Section VII presents the experimental results and their analysis. Finally, Section VIII presents the conclusions of the study.

## II. Related Works

Recent studies have explored optimization-based approaches for IIR filter design using various techniques, including particle swarm optimization (PSO) [15], which leverages swarm intelligence for global search; multi-objective evolutionary algorithms [16], [17], which optimize multiple conflicting objectives simultaneously; differential evolution (DE) [18], [19], [20], recognized for its balance between exploration and exploitation through mutation and recombination; and sparse linear programming [21], which enforces sparsity constraints to reduce computational complexity. Among these methods, differential evolution has received considerable attention in IIR filter design due to its strong global search capabilities, computational efficiency, and straightforward implementation.

Both Chen et al. [19] and Chen et al. [20] utilize the AMECoDEs algorithm to optimize IIR digital filter design by evolving both structure and coefficients. Chen et al. [19] introduce a subsystem-based structure evolution approach, demonstrating superior performance and faster convergence compared to five state-of-the-art algorithms. Additionally, this method ensures filter stability by maintaining poles within the unit circle. This work focuses on the design of classical IIR filters. Building on this approach, Chen et al. [20] extend the method to dual-passband digital filters, achieving notable improvements in passband ripple, stopband attenuation, and convergence speed compared to previous optimization techniques. A comparative summary is presented in Table I, highlighting the features of optimization approaches for IIR filter design in related works.

Multiple-passband digital filters are widely utilized in various fields, including communications [22] and biomedical signal processing [23]. Consequently, the design of such multiband filters has been an area of research interest for several years. Previous research has explored various methodologies for multiband filter design, employing distinct approaches. In [24], an optimal equiripple FIR filter design method was introduced for triple narrow bandpass and triple narrow notch filters, ensuring Chebyshev-optimal performance. Xiao et al. [25] proposed a fast design technique for multiband IIR filters with a general Chebyshev characteristic, enabling precise control over bandwidths and ripples without increasing filter order. In [26], an algebro-geometric approach was developed to synthesize optimal multiband filters with the lowest possible order, narrow transition bands, and high stopband attenuation. More recently, Wu et al. [27] introduced the DST-O method, a hybrid analytical-optimization approach for multiband IIR filter design, leveraging direct synthesis techniques from analog Chebyshev filters combined with optimization to achieve equal ripple in all passbands.

Building on these advancements, this study extends the scope of IIR filter design beyond classical and dual-passband configurations by introducing the design of triple-passband IIR filters. It emphasizes the effectiveness of differential evolution as an optimization technique, achieving improved stopband attenuation and employing a constant weight function in MSE calculation, rather than the conventional piecewise linear weight function, to enhance filter performance. Table II presents a comparative analysis of design methods for multiband digital filters, revealing that all approaches listed in the table rely on conventional or hybrid design methodologies, whereas our proposed approach is based purely on optimization.

### A. Research Gap

To the best of our knowledge, no prior studies have compared the AMECoDEs and FDDE algorithms in designing IIR digital filters to assess their applicability to this problem. Although both algorithms have been used successfully in various optimization tasks, their performance in this context remains unexplored.

Although differential evolution has been successfully applied to classical and dual-passband IIR filters, its potential for more complex designs, such as triple-passband filters, remains largely unexplored, creating a gap in the optimization of higher-order multiband filters.

Moreover, the performance evaluation of IIR filter designs using evolutionary algorithms typically relies on a piecewise linear function. While this approach provides adaptability in certain scenarios, it does not necessarily yield optimal performance in all applications. The impact of employing a constant weight function within each frequency band has not been thoroughly investigated.

## III. Differential Evolution

Differential Evolution (DE), originally introduced by Rainer Storn and Kenneth Price [28], is a global optimization

TABLE I. COMPARISON OF FEATURES OF OPTIMIZATION APPROACHES FOR IIR FILTER DESIGN IN RELATED WORKS

| Feature | Chen et al. [19] | Chen et al. [20] | This Work |
|---|---|---|---|
| **Optimization Algorithms** | AMECoDEs | AMECoDEs | AMECoDEs, FDDE |
| **IIR Filter Type** | Classical | Dual-passband | Classical, Dual-passband, Triple-passband |
| **Structure Evolution** | Yes (subsystem-based) | Yes (subsystem-based) | No |
| **Passband Ripple** | Low | Low | Comparable or better |
| **Stopband Attenuation** | Good | Good | Improved |
| **Weight Function** | Linear piecewise | Linear piecewise | Constant weight function within each frequency band |

TABLE II. COMPARISON OF DESIGN METHODS FOR MULTIBAND DIGITAL FILTERS

| Reference | Method Name | Main Characteristic | Design Type |
|---|---|---|---|
| **Zahradnik et al. [24]** | Equiripple FIR Design | Optimizes triple narrow bandpass and notch filters in the Chebyshev sense. | Conventional |
| **Xiao [25]** | Chebyshev-Based Multiband Mapping | Enables precise control of bandwidths and ripples without increasing filter order, using transmission zeros. | Conventional |
| **Bogatyrev et al. [26]** | Algebro-Geometric Synthesis | Designs multiband filters with the lowest possible order, narrow transition bands, and high stopband attenuation. | Conventional |
| **Wu et al. [27]** | DST-O Method | Combines direct synthesis from analog Chebyshev filters with optimization to achieve equal ripple in all passbands. | Hybrid (Conventional + Optimization) |

technique based on biological evolution, employing mutation, crossover, and natural selection to explore optimal solutions in a multi-dimensional search space. Recent advancements in differential evolution algorithms have enhanced the precision and efficiency of objective function optimization [29]. Consequently, these algorithms have been successfully applied in diverse fields, including neural networks [30], [31], control and automation [32], [33], [34], wireless communications [35], [36], and remote sensing [37].

The term "Differential Evolution" is used because it employs differential vectors to guide the search towards better solutions. A differential vector is the difference between two solution vectors in the search space. The basic differential evolution process can be described in the following steps: initialization, differential mutation, crossover, and selection.

In the initialization step, an initial population of random solution vectors is generated within the defined search space. A population of individuals in generation $G$ is represented as $\mathbf{X}^G = \{X_1^G, X_2^G, \ldots, X_{NP}^G\}$. An individual in the population with index $i$ in generation $G$ is represented as ${X_i}^G = \{x_{i,1}^G, x_{i,2}^G, \ldots, x_{i,D}^G\}$, $(i = 1, 2, \ldots, NP)$, where $NP$ is the population size, and $D$ is the dimension of the objective function.

Differential mutation involves generating a mutated vector ${V_i}^G = \{v_{i,1}^G, v_{i,2}^G, \ldots, v_{i,D}^G\}$ for each individual in the population by combining different solutions from the current population through the addition of a differential vector, multiplied by a scale factor, with a selected target solution vector. The mutated vectors form a population represented as $\mathbf{V}^G = \{V_1^G, V_2^G, \ldots, V_{NP}^G\}$. In [38], several mutation strategies are mentioned, of which we describe the following two most commonly used: DE/rand/1 and DE/best/1.

The DE/rand/1 strategy is based on the equation:

$$V_i^G = X_{r1}^G + F \times (X_{r2}^G - X_{r3}^G) \tag{2}$$

The DE/best/1 strategy is described as:

$$V_i^G = X_{best}^G + F \times (X_{r1}^G - X_{r2}^G) \tag{3}$$

where $V_i^G$ is the mutated vector; $X_i^G$ is the individual with index $i$ in generation $G$; $X_{best}^G$ is the best individual in generation $G$; $F$ is the scale factor; $r1$, $r2$, and $r3$ are indices in the range $[1, NP]$ such that $r1 \neq r2 \neq r3 \neq i$.

Crossover is performed to introduce genetic diversity into the population. For each individual in the population, a trial vector $U_i^G = \{u_{i,1}^G, u_{i,2}^G, \ldots, u_{i,D}^G\}$ is generated by combining each target vector $X_i^G$ with its corresponding mutated vector $V_i^G$ based on the following equation:

$$u_{i,k}^G = \begin{cases} v_{i,k}^G, & \text{if } rand_{i,k}(0,1) \leq CR \text{ or } k = k_{rand} \\ x_{i,k}^G & \text{otherwise} \end{cases} \tag{4}$$

where $rand_{i,k}(0,1)$ generates a random number in the range $[0,1]$, $CR$ is the crossover rate, and $k_{rand}$ is an integer random value in the range $[1, D]$ that ensures $U_i^G$ is different from $X_i^G$. The trial vectors form a population represented as $\mathbf{U}^G = \{U_1^G, U_2^G, \ldots, U_{NP}^G\}$.

In the selection stage, the trial vector $U_i^G$ is compared to the target solution vector $X_i^G$, and the better one is selected to be part of the population in the next generation according to the equation:

$$X_i^{G+1} = \begin{cases} U_i^G, & \text{if } f(U_i^G) \leq f(X_i^G) \\ X_i^G & \text{otherwise} \end{cases} \tag{5}$$

where $f(X_i^G)$ and $f(U_i^G)$ are the fitness values of the target solution vector and its trial vector, respectively. This process is repeated for all individuals in the population. The replacement process ensures that only the most promising solutions are retained in each generation.

The mutation, crossover, and selection steps are repeated for several generations until a termination criterion is met, such as reaching a maximum number of generations or achieving an acceptable optimal solution.

Differential evolution has various variants and adjustable parameters, such as population size, mutation and crossover

strategies, and selection criteria. These parameters influence the balance between exploration and exploitation of the search space, allowing the technique to be adapted to different types of problems and application domains.

One notable variant of differential evolution is the AMECoDEs algorithm, developed by Laizhong Cui et al. and introduced in [39]. This algorithm enhances differential evolution through two key mechanisms. The first is multiple elite-guided mutation, where each individual is influenced simultaneously by two elite solutions, reducing the risk of deception by suboptimal regions. The second is the shift mechanism, designed to mitigate premature convergence and stagnation. By integrating these strategies, AMECoDEs aims to address these issues more effectively than single-elite mutation approaches. Notably, AMECoDEs has recently been applied to the design of IIR digital filters [19] [20].

Another recent variant of differential evolution is the Differential Evolution Algorithm with Fitness and Diversity Ranking-Based Mutation Operator (FDDE), proposed by Jianchao Cheng et al. in [40]. FDDE estimates population diversity based on fitness values, thereby reducing computational overhead. By combining fitness ranking with diversity ranking, it establishes a final ranking that guides the mutation process. This approach ensures an adaptive balance between exploration and exploitation by strategically assigning positions to individuals during mutation. In [40], the authors present experimental results demonstrating the superiority of FDDE over advanced DE variants, including jDE, rank-jDE, SHADE, and L-SHADE, across a range of global optimization benchmarks involving both low- and high-dimensional problems. Given the demonstrated effectiveness of both AMECoDEs and FDDE in optimization tasks, this study compares their performance in the design of IIR digital filters.

Luo et al. [41] recently introduced an enhanced DE algorithm with a hierarchical selection mutation strategy and a distance-based probabilistic selection approach, demonstrating competitive performance across multiple benchmark functions and real-world problems. The recent publication of their work highlights the ongoing interest of the scientific community in the development of advanced Differential Evolution algorithms.

## IV. Problem Statement

The general problem in the design of a classic digital filter involves determining the coefficients of the transfer function in Eq. (1) so that the magnitude of the filter's frequency response meets the specifications outlined in a tolerance scheme. This scheme defines the passbands, stopbands, and transition bands, along with the maximum errors allowed in the passbands and stopbands. Typically, there are no specific requirements for the transition bands.

When designing digital filters using evolutionary algorithms, the problem revolves around given the desired magnitude response $|H_d(\omega)|$, finding the coefficients of the filter's transfer function that correspond to a magnitude response as close as possible to the desired one. To quantify how well the designed filter's magnitude response approximates the desired magnitude response, the mean squared error (MSE) is frequently used [42], [43], [44]. Generally, the evolutionary process seeks to minimize the mean squared error.

In this study, the input to the IIR digital filter design procedure is the desired magnitude response, while the output is the optimal filter obtained at the conclusion of the evolutionary process. Table III presents the passbands ($|H_d(\omega)| = 1$) and stopbands ($|H_d(\omega)| = 0$) of the filters to be designed, expressed in normalized frequency units. In this normalization, the sampling frequency $f_s$ is mapped to $2\pi$. The considered filter types include classical low-pass, high-pass, band-pass, and band-stop filters, as well as symmetrical and asymmetrical dual-passband and triple-passband filters.

The frequency specifications for the asymmetrical triple-passband filter, as listed in Table III, are as follows: The filter features three passbands: $[0.1\pi, 0.2\pi]$, $[0.4\pi, 0.5\pi]$ and $[0.7\pi, 0.9\pi]$; four stopbands: $[0, 0.05\pi]$, $[0.25\pi, 0.35\pi]$, $[0.55\pi, 0.65\pi]$, and $[0.95\pi, \pi]$; and six transition bands: $(0.05\pi, 0.1\pi)$, $(0.2\pi, 0.25\pi)$, $(0.35\pi, 0.4\pi)$, $(0.5\pi, 0.55\pi)$, $(0.65\pi, 0.7\pi)$, and $(0.9\pi, 0.95\pi)$.

In this work, each filter type specified in Table III was designed using the differential evolution algorithms FDDE and AMECoDEs. The performance of these filters was then evaluated based on the mean squared error of their magnitude responses. To ensure a fair comparison, the implementations of the FDDE and AMECoDEs algorithms for IIR digital filter design operated under uniform general conditions, including identical filter representation, the same fitness evaluation algorithms, and identical weight functions.

Subsequently, the classic and dual-passband filters designed in this work were compared with IIR filters presented in two recent studies [19], [20]. However, since not all general conditions were identical in this case, the comparison was based on the characteristics of the filters' magnitude responses. Finally, the designed triple-passband filters were experimentally validated using a development board.

In the following section, the FDDE algorithm applied to the design of IIR digital filters is described. The AMECoDEs algorithm is not detailed, as it has already been applied for this purpose in [19] and [20].

## V. FDDE Algorithm for the Design of IIR Digital Filters

The FDDE algorithm, described in this section, was originally introduced by Cheng et al. [40]. This algorithm has been adapted for the evolution of IIR digital filters, as shown in Algorithm V.

The algorithm begins by randomly generating an initial population, $\mathbf{X}^0$, consisting of $NP$ filters, as described in subsection VI-B. Next, the fitness of each filter is evaluated. The evolutionary process then iterates until the maximum number of generations $(MNG)$ is reached. During each iteration, the following operations are performed:

- The final ranking of the filters in the population $\mathbf{X}^G$ is determined.
- The filters are sorted in ascending order according to the final ranking.

TABLE III. DESIRED MAGNITUDE RESPONSE OF THE DESIGNED FILTERS

| Filter class | Filter type | Band ($\pi$) | | $\lvert H_d(\omega)\rvert$ |
|---|---|---|---|---|
| | | *From* | *To* | |
| Classic filters | Low-pass | 0 | 0.45 | 1 |
| | | 0.5 | 1 | 0 |
| | High-pass | 0 | 0.3 | 0 |
| | | 0.35 | 1 | 1 |
| | Band-pass | 0 | 0.3 | 0 |
| | | 0.35 | 0.65 | 1 |
| | | 0.7 | 1 | 0 |
| | Band-stop | 0 | 0.3 | 1 |
| | | 0.35 | 0.65 | 0 |
| | | 0.7 | 1 | 1 |
| Multiple-passband filters | Symmetrical dual-passband | 0 | 0.05 | 0 |
| | | 0.15 | 0.35 | 1 |
| | | 0.45 | 0.55 | 0 |
| | | 0.65 | 0.85 | 1 |
| | | 0.95 | 1 | 0 |
| | Asymmetrical dual-passband | 0 | 0.05 | 0 |
| | | 0.15 | 0.45 | 1 |
| | | 0.55 | 0.65 | 0 |
| | | 0.75 | 0.85 | 1 |
| | | 0.95 | 1 | 0 |
| | Symmetrical triple-passband | 0 | 0.05 | 0 |
| | | 0.1 | 0.2 | 1 |
| | | 0.25 | 0.35 | 0 |
| | | 0.4 | 0.6 | 1 |
| | | 0.65 | 0.75 | 0 |
| | | 0.8 | 0.9 | 1 |
| | | 0.95 | 1 | 0 |
| | Asymmetrical triple-passband | 0 | 0.05 | 0 |
| | | 0.1 | 0.2 | 1 |
| | | 0.25 | 0.35 | 0 |
| | | 0.4 | 0.5 | 1 |
| | | 0.55 | 0.65 | 0 |
| | | 0.7 | 0.9 | 1 |
| | | 0.95 | 1 | 0 |

- For each filter $X_i^G$, the following operations are performed: The mutated filter $V_i^G$ is obtained (Line 7 in Algorithm V), the trial filter $U_i^G$ is obtained through the crossover operation between $X_i^G$ and $V_i^G$ (Lines 8-15 in Algorithm V). The fitness of the trial filter $U_i^G$ is calculated, which is compared to the fitness of $X_i^G$, and the filter with the lower fitness is retained for the next generation (Lines 17-23 in Algorithm V).
- The number of generation is updated: $G = G + 1$.

In Algorithm V, for each value of $i$ and $k$, the function $rand_{i,k}(0,1)$ generates a random real number in the interval $[0,1]$. The function $rand(1,D)$ produces a random integer in the interval $[1,D]$, where $D$ is the number of second-order sections, and $CR$ is the crossover rate. The representations $x_{i,k}^G$, $v_{i,k}^G$, $u_{i,k}^G$ $(k = 1,2,\ldots,D)$ are the second-order sections that make up the filters $X_i^G$, $V_i^G$, $U_i^G$, respectively.

### A. Final Ranking Evaluation

The FDDE algorithm, before performing the mutation operation, requires that the population be sorted according to the final ranking. In [40], the final ranking is referred to as the combination of fitness ranking and diversity ranking. Below, we describe the process of obtaining the final ranking:

**Algorithm 1:** The FDDE Algorithm for IIR Filter Design Adapted from [40]

**Input:** $|H_d(\omega_n)|$ is the desired magnitude response $(n = 0,1,2,\ldots,N-1)$
**Output:** $X_{best}$ is the best-found filter with fitness $f_{best}$
**Data:** $w_n$ is the weight vector $(n = 0,1,2,\ldots,N-1)$

1 Generate an initial filter population randomly $\mathbf{X}^0 = \{X_1^0, X_2^0, \ldots, X_{NP}^0\}$ and set the generation $G = 0$;
2 Evaluate fitness value $f_i = f(X_i^0)\ \ (i = 1,2,\ldots,NP)$;
3 **while** $(G < MNG)$ **do**
4  Calculate the final ranking of each filter in population $\mathbf{X}^G$ according to subsection V-A ;
5  Sort population $\mathbf{X}^G$ in ascending order according to final ranking;
6  **for** $i = 1$ *to* $NP$ **do**
7  For each filter $X_i^G$, obtain the mutated filter $V_i^G$ according to subsection V-B;
8  Generate an integer number randomly $k_{rand} = rand(1,D)$;
9  **for** $k = 1$ *to* $D$ **do**
10  **if** $rand_{i,k}(0,1) \le CR$ *or* $k = k_{rand}$ **then**
11  $u_{i,k}^G = v_{i,k}^G$;
12  **end**
13  **else**
14  $u_{i,k}^G = x_{i,k}^G$;
15  **end**
16  **end**
17  Evaluate fitness value $f(U_i^G)$;
18  **if** $f({U_i}^G) \le f({X_i}^G)$ **then**
19  ${X_i}^{G+1} = {U_i}^G$;
20  **end**
21  **else**
22  ${X_i}^{G+1} = {X_i}^G$;
23  **end**
24  **end**
25  $G = G + 1$;
26 **end**

The filters in population $\mathbf{X}^G$ are arranged in ascending order based on their fitness. Then, the fitness ranking is computed using the equation:

$$FR_i = i, \ \ (i = 1,2,...,NP) \tag{6}$$

Before calculating the deviation for each filter, the filter whose fitness ranking is $FR_i = NP/2$ is determined, and the value of its fitness is denoted as $f_{mid}$. Then, for each filter in the population, the deviation is calculated using the equation:

$$f_{de,i} = |f_i - f_{mid}|, \ \ (i = 1,2,...,NP) \tag{7}$$

After sorting the population in ascending order based on deviation, the diversity ranking for each filter is calculated using the equation:

$$DR_i = NP - i, \quad (i = 1, 2, ..., NP) \tag{8}$$

Finally, the fitness ranking and diversity ranking are combined to obtain the final ranking using the equation:

$$R_i = w \times DR_i + (1 - w) \times FR_i, \quad (i = 1, 2, ..., NP) \tag{9}$$

where $w = \frac{G}{MNG}$. In this expression, $G$ is the current generation number, and $MNG$ is the maximum number of generations. It can be observed that, according to Eq. (9), in the early generations of the evolutionary process, the final ranking depends more on the fitness ranking, and in the later generations, it depends more on the diversity ranking. The name of the FDDE algorithm is precisely because the mutation operation depends on the final ranking.

### B. Mutation Operation

For each filter $X_i^G$, the mutation operation is performed using the "DE/rand/1" strategy, for which the integer values $r1$, $r2$, and $r3$ are randomly selected within the range $[1, NP]$ such that $r1 \neq r2 \neq r3 \neq i$, and the filters $X_{r1}^G$, $X_{r2}^G$, $X_{r3}^G$ are sorted in ascending order based on their final ranking values $R_{r1}$, $R_{r2}$, $R_{r3}$. If the sorted filters are represented as $X_{t1}^G$, $X_{t2}^G$, $X_{t3}^G$, then the mutated filter $V_i^G$ is calculated using the following equation:

$$V_i^G = X_{t1}^G + F \times (X_{t2}^G - X_{t3}^G) \tag{10}$$

where the scale factor $F$, with a probability of $CFP = 0.7$, is a fixed value equal to $CF = 0.5$; and with a probability of $1 - CFP = 0.3$, is equal to $4 \times (factor - 0.5)$, where $factor$ is a random real number in the range from 0 to 1.

## VI. Methodology

This section outlines the approach employed for designing IIR digital filters using the differential evolution algorithms FDDE and AMECoDEs. Specifically, it details the representation of the IIR filter structure, the initialization of candidate solutions, the formulation of the fitness function, the applied weight function, the determination of $C_{\text{stop}}$, and the construction of the comparative table.

### A. Filter Representation

A digital IIR filter is represented as a serial connection of second-order sections (SOS). This representation is employed in various models and applications, for instance, in the works [45], [46], IIR filters are implemented in FPGA using this representation.

The transfer function of the filter $X_i^G$, belonging to the population $\mathbf{X}^G = \{X_1^G, X_2^G, \ldots, X_{NP}^G\}$, is expressed as the product of the transfer functions of the second-order sections, as shown in the equation:

$$H_{X_i^G}(z) = \prod_{k=1}^{D} \frac{b_{i,k,0}^G + b_{i,k,1}^G \cdot z^{-1} + b_{i,k,2}^G \cdot z^{-2}}{1 + a_{i,k,1}^G \cdot z^{-1} + a_{i,k,2}^G \cdot z^{-2}} \tag{11}$$

where $D$ is the number of sections.

To describe mutation and crossover operations, the IIR filter $X_i^G$ ($i$ is the index within the filter population) is represented through its second-order sections in matrix form as follows:

$$X_i^G = \begin{bmatrix} x_{i,1}^G \\ x_{i,2}^G \\ \vdots \\ x_{i,D}^G \end{bmatrix} = \begin{bmatrix} b_{i,1,0}^G & b_{i,1,1}^G & b_{i,1,2}^G & 1 & a_{i,1,1}^G & a_{i,1,2}^G \\ b_{i,2,0}^G & b_{i,2,1}^G & b_{i,2,2}^G & 1 & a_{i,2,1}^G & a_{i,2,2}^G \\ \vdots & \vdots & \vdots & \vdots & \vdots & \vdots \\ b_{i,D,0}^G & b_{i,D,1}^G & b_{i,D,2}^G & 1 & a_{i,D,1}^G & a_{i,D,2}^G \end{bmatrix} \tag{12}$$

where $x_{i,k}^G$ represents the second-order section with index $k$ with numerator polynomial coefficients $b_{i,k,0}^G$, $b_{i,k,1}^G$, $b_{i,k,2}^G$ and denominator polynomial coefficients 1, $a_{i,k,1}^G$, $a_{i,k,2}^G$.

In this work, throughout the evolutionary process, each second-order section is generated and maintained as a stable system. This implies that the poles of the transfer function for the second-order section remain within the unit circle. Consequently, if during the mutation operation, the distance $r$ from a pole to the origin exceeds 1, its magnitude is adjusted using the following equation while preserving its angle:

$$1 - (1/r) \tag{13}$$

### B. Initial Filter Population

Each filter in the initial filter population ($G = 0$) is generated in the following way:

In each second-order section $x_{i,k}^0$, the numerator polynomial coefficients are real random numbers with an absolute value less than or equal to 1, determined by the equation:

$$\begin{aligned} b_{i,k,0}^0 &= rand(-1, 1); \\ b_{i,k,1}^0 &= rand(-1, 1); \\ b_{i,k,2}^0 &= rand(-1, 1) \end{aligned} \tag{14}$$

The denominator polynomial coefficients of $x_{i,k}^0$ are obtained from a complex number $re^{j\varphi}$, which is one of the roots of the polynomial, using operations that ensure the second-order section is stable:

$$\begin{aligned} r = rand(0, 1),\ 0 \leq r < 1;\ \varphi = rand(-\pi, \pi); \\ ; a_{i,k,0}^0 = 1;\ a_{i,k,1}^0 = -2r \cdot cos(\varphi);\ a_{i,k,2}^0 = r^2 \end{aligned} \tag{15}$$

**Algorithm 2:** IIR Filter Fitness Evaluation

**Input:** $X_i^G$ is the digital IIR filter represented in terms of second-order sections.
**Output:** Filter fitness $f(X_i^G)$.
**Data:** $\omega = \{\omega_n\}$ is the frequency vector, $|H_d(\omega_n)|$ is the desired magnitude response, $w_n$ is the weight vector $(n = 0, 1, ..., N-1)$, $X_{best}$ is the best-found filter, $f_{best}$ is the fitness of the best-found filter.

Calculate the frequency response of the filter $H_{X_i^G}(\omega_n)$ $(n = 0, 1, ..., N-1)$ using Eq. (16);
Calculate the fitness $f(X_i^G)$ as the mean squared error using Eq. (17);
**if** $f(X_i^G) < f_{best}$ **then**
  $X_{best} = X_i^G$, $f_{best} = f(X_i^G)$;
**end**

### C. Fitness Evaluation

In this work, as the fitness function of an IIR filter, we employ the Weighted Mean Squared Error (WMSE) of the filter's magnitude response in comparison to the desired magnitude response. Henceforth, we will simply refer to it as the Mean Squared Error (MSE).

To determine the fitness of a digital IIR filter, it is necessary to define the discrete-time frequencies at which the frequency response will be evaluated. We set up $N$ equally spaced frequencies in the interval from 0 to $\pi$, forming the set $\omega = \{\omega_n\} = \{\frac{\pi\, n}{N-1}\}$ $(n = 0, 1, ..., N-1)$. $N$ is the number of sampling points.

Given a digital IIR filter $X_i^G$, its frequency response at the frequencies in the set $\omega$ is calculated as the product of the frequency responses of the second-order sections using the equation:

$$H_{X_i^G}(\omega_n) = \prod_{k=1}^{D} \frac{b_{i,k,0}^G + b_{i,k,1}^G \cdot e^{-j\omega_n} + b_{i,k,2}^G \cdot e^{-2j\omega_n}}{1 + a_{i,k,1}^G \cdot e^{-j\omega_n} + a_{i,k,2}^G \cdot e^{-2j\omega_n}}, \quad (n = 0, 1, ..., N-1) \tag{16}$$

The mean squared error of the filter's magnitude response $X_i^G$ is calculated using the equation:

$$f(X_i^G) = \frac{1}{N} \sum_{n=0}^{N-1} w_n \cdot (\left|H_{X_i^G}(\omega_n)\right| - |H_d(\omega_n)|)^2 \tag{17}$$

where $|H_d(\omega_n)|$ is the desired magnitude response at frequency $\omega_n$. The values $w_n$ $(n = 0, 1, \ldots, N-1)$ constitute the weight function.

The fitness evaluation procedure is outlined in Algorithm VI-C. In the final step, each time the fitness of a filter is calculated, the result is compared to the fitness of the best-found filter. If the obtained result is lower, then the best-found filter is updated.

### D. Weight Function

The weight function, denoted as $w_n$ in Eq. (17), represents a sequence of values utilized for assigning varying degrees of significance to the mean square errors associated with individual frequencies, $\omega_n$.

In the works [19], [20], the weights follow a discrete linear piecewise function with peak values at frequencies 0, $\pi$, and at the centers of transition bands; and with minimum values at the centers of passbands and stopbands. In these studies, the authors contend that the linearity of the weight function ensures that the weights of neighboring sampling points change gradually, without discontinuities, as a sharp change in the weights leads to a significant variation in the magnitude response.

In the present study, a simple weight function has been employed, which remains constant within each band. To prevent substantial changes in the magnitude response, the weight corresponding to the suppression bands has been experimentally selected. The weights used are: In the transition bands, it is $w_n = C_{\text{tran}} = 0$, as there is no specific requirement within these bands. In the passbands, it is $w_n = C_{\text{pass}} = 1$, as we aim for the designed filter to closely match the desired magnitude response within these bands. In the stopbands, a value $w_n = C_{\text{stop}}$ greater than 1 is chosen to indicate the importance of attenuation within these bands, and non-compliance with this specification is penalized.

### E. Determination of $C_{stop}$ and Comparative Table Generation

For each filter type specified in Table III, the following stages were carried out:

Utilizing the constant piecewise weight function with $w_n = C_{\text{tran}} = 0$, $w_n = C_{\text{pass}} = 1$, and $w_n = C_{\text{stop}}$, the design program based on the FDDE algorithm was executed for five different values of $C_{\text{stop}}$, which were empirically adjusted. Given the probabilistic nature of the evolutionary process, the program was run ten times for each $C_{\text{stop}}$ value, and the solution with the lowest mean square error was selected from the ten outcomes. To determine a final filter among the five designed for different $C_{\text{stop}}$ values, the primary selection criterion was to maximize the minimum attenuation in the stopbands while maintaining relatively low passband ripple. Table IV presents the evaluated values of $C_{\text{stop}}$ along with the selected value for each filter type.

With $C_{\text{pass}} = 1$, $C_{\text{tran}} = 0$, and the $C_{\text{stop}}$ value, selected in the previous stage, the design program using the AMECoDEs algorithm has been executed 10 times. The result with the lowest mean square error was selected from the 10 outcomes.

The mean square error of the magnitude response obtained with the AMECoDEs algorithm in the previous stage has been compared to that obtained with the FDDE algorithm. The comparison is detailed in Table V.

## VII. Experimental Results and Discussion

### A. Comparison of Filters Designed using the FDDE and AMECoDEs Algorithms

Table V indicates that both algorithms produce identical MSE values for low-pass and band-stop filters. For high-pass

TABLE IV. EVALUATED AND SELECTED $C_{STOP}$ VALUES FOR EACH FILTER TYPE

| Filter type | $C_{stop}$ | | | | | Selected value |
|---|---|---|---|---|---|---|
| Low-pass | 300 | 500 | 700 | 900 | 1100 | 1100 |
| High-pass | 300 | 500 | 700 | 900 | 1100 | 1100 |
| Band-pass | 3 | 4 | 5 | 6 | 7 | 4 |
| Band-stop | 4 | 8 | 12 | 16 | 20 | 12 |
| Symmetric dual-passband | 4 | 8 | 12 | 16 | 20 | 12 |
| Asymmetric dual-passband | 4 | 8 | 12 | 16 | 20 | 16 |
| Symmetric triple-passband | 20 | 30 | 40 | 50 | 60 | 60 |
| Asymmetric triple-passband | 20 | 30 | 40 | 50 | 60 | 40 |

TABLE V. COMPARISON OF MEAN SQUARED ERROR FOR FILTERS DESIGNED USING THE FDDE AND AMECODES ALGORITHMS

| Filter class | Filter type | MSE | | Best |
|---|---|---|---|---|
| | | *FDDE* $\times 10^{-4}$ | *AMECoDEs* $\times 10^{-4}$ | |
| Classic filters | Low-pass | 1.11480 | 1.11480 | = |
| | High-pass | 0.53937 | 0.53939 | FDDE |
| | Band-pass | 4.84230 | 6.10280 | FDDE |
| | Band-stop | 8.94030 | 8.94030 | = |
| Multiple-passband filters | Symmetrical dual-passband | 0.51522 | 0.47240 | AMECoDEs |
| | Asymmetrical dual-passband | 1.04140 | 0.17376 | AMECoDEs |
| | Symmetrical triple-passband | 43.00300 | 11.05200 | AMECoDEs |
| | Asymmetrical triple-passband | 21.52700 | 7.90040 | AMECoDEs |

and band-pass filters, the FDDE algorithm exhibits a slight improvement. In contrast, the AMECoDEs algorithm demonstrates marginally better performance for the symmetric dual-passband filter. Notably, AMECoDEs achieves a significantly lower MSE for the asymmetric dual-passband filter, as well as for both symmetric and asymmetric triple-passband filters.

The magnitude response curves of the designed filters are presented in Fig. 1 to 8. It is observed that, for low-pass, high-pass, band-stop, and symmetric dual-passband filters, the curves generated by the AMECoDEs and FDDE algorithms display a high degree of similarity. The curve of the band-pass filter designed with FDDE algorithm is better than the one designed with AMECoDEs algorithm. However, the curves of the asymmetric dual-passband and the both symmetric and asymmetric triple-passband filters designed with AMECoDEs algorithm exhibit significantly better attenuation in the stop-bands.

### *B. Comparison of the Designed Filters with Previous Studies*

The filters designed in this study using the FDDE and AMECoDEs algorithms have been compared with those presented in [19] (classic filters) and [20] (dual-passband filter). The design conditions in these prior works do not fully align with those employed in our research. For instance, the previous studies utilized optimized structures and a piecewise discrete linear weight function. As a result, the comparison was

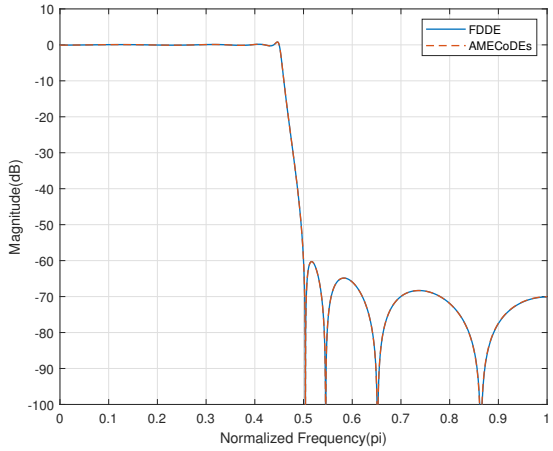


Fig. 1. Magnitude response of the low-pass filter designed using FDDE and AMECoDEs algorithms.

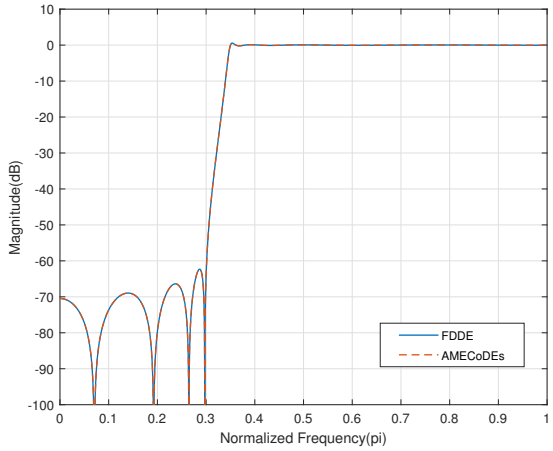


Fig. 2. Magnitude response of the high-pass filter designed using FDDE and AMECoDEs algorithms.

conducted based on the magnitude response characteristics of the filters, as shown in Tables VI and VII.

In these tables, "AMECoDEs 1" refers to the filter designed in [19] or [20], while "AMECoDEs 2" and "FDDE" denote the filters developed in this study using the respective algorithms. It is important to highlight that AMECoDEs 1 and AMECoDEs 2 originate from the same evolutionary algorithm but differ in the specific conditions and parameters applied during their design. Therefore, rather than referring to them as distinct algorithms, they will be considered different design approaches in this comparison.

In Table VI, it can be observed that in the high-pass filter and the band-stop filter, the passband ripples, represented as $\delta_{pass}$, of the filters designed with AMECoDEs 2 and FDDE approaches are slightly smaller compared to the filters designed with AMECoDEs 1 approach, while in the low-pass filter and the band-pass filter, they are larger. The widths of the transition bands, represented as $\Delta\omega$, are slightly smaller in most cases with the AMECoDEs 2 and FDDE approaches. In

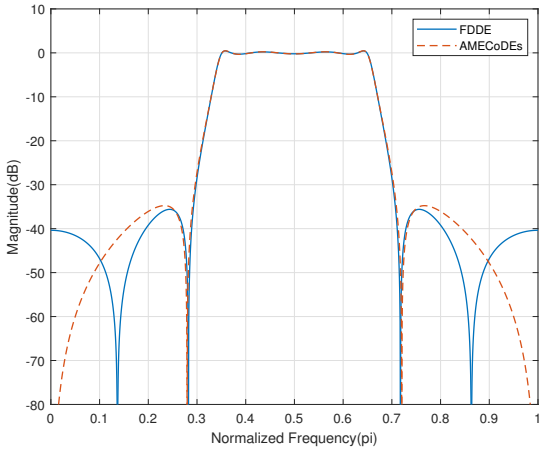


Fig. 3. Magnitude response of the band-pass filter designed using FDDE and AMECoDEs algorithms.

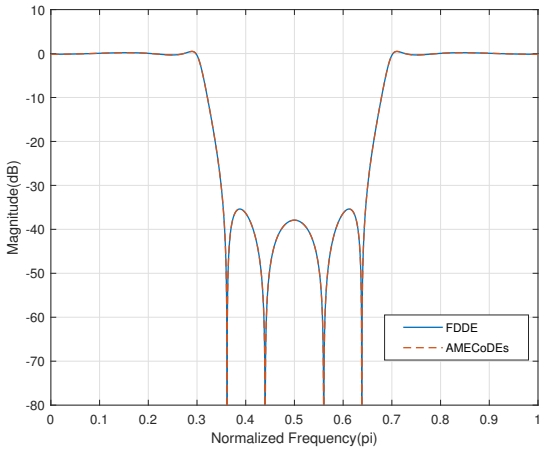


Fig. 4. Magnitude response of the band-stop filter designed using FDDE and AMECoDEs algorithms.

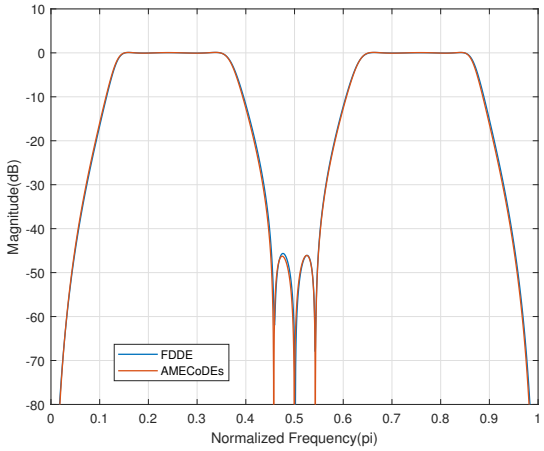


Fig. 5. Magnitude response of the symmetrical dual-passband filter designed using FDDE and AMECoDEs algorithms.

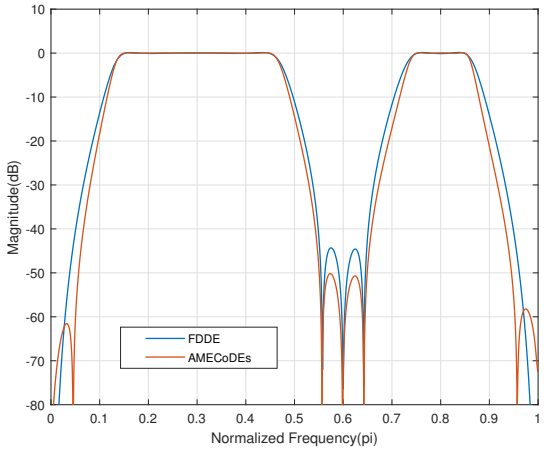


Fig. 6. Magnitude response of the asymmetrical dual-passband filter designed using FDDE and AMECoDEs algorithms.

almost all cases, the attenuation in the stopbands, denoted as $A_{stop}$, of the filters obtained with AMECoDEs 2 and FDDE approaches is approximately 5dB higher compared to the stopband attenuation of the filters obtained with AMECoDEs 1 approach. Similarly, from Table VII, it is clear that the ripple values in the passbands of the dual-passband filters are smaller with the AMECoDEs 2 and FDDE approaches, except for the ripple in passband 2 of the asymmetric dual-passband filter, where it is larger with FDDE approach. Additionally, the attenuation values in all stopbands are higher by 13dB with the AMECoDEs 2 and FDDE approaches compared to those obtained with AMECoDEs 1 approach.

Table VI reveals that for the high-pass and band-stop filters, the passband ripple is slightly lower in the filters designed using the AMECoDEs 2 and FDDE approaches compared to those designed with the AMECoDEs 1 approach. Conversely, for the low-pass and band-pass filters, the passband ripple is slightly higher. The transition band widths tend to be marginally narrower in most cases when employing the AMECoDEs 2 and FDDE approaches. Moreover, in nearly all cases, the stopband attenuation of filters designed using the AMECoDEs 2 and FDDE approaches is approximately 5 dB higher than that of filters obtained with the AMECoDEs 1 approach.

Similarly, Table VII indicates that the passband ripple of dual-passband filters is generally lower when using the AMECoDEs 2 and FDDE approaches, with the exception of passband 2 in the asymmetric dual-passband filter, where the ripple is higher when employing the FDDE approach. Furthermore, the attenuation in all stopbands is consistently higher by 13 dB in filters designed using the AMECoDEs 2 and FDDE approaches compared to those obtained with the AMECoDEs 1 approach.

The parameters of the AMECoDEs 1, AMECoDEs 2, and FDDE approaches are presented in Table VIII. One can observe that the parameters of AMECoDEs 2 and FDDE are largely similar, except for those specific to the AMECoDEs algorithm, which are absent in FDDE. In Table VIII, $p$, $c$,

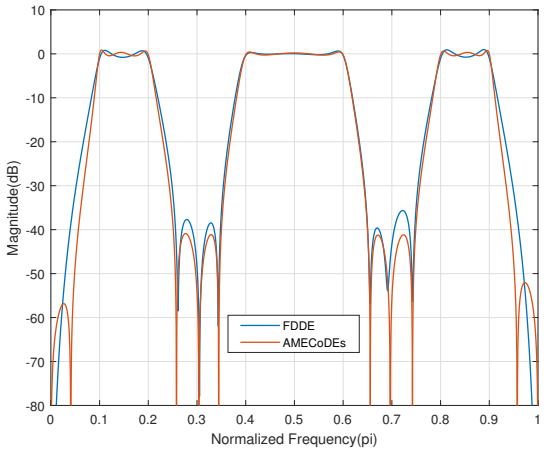


Fig. 7. Magnitude response of the symmetrical triple-passband filter designed using FDDE and AMECoDEs algorithms.

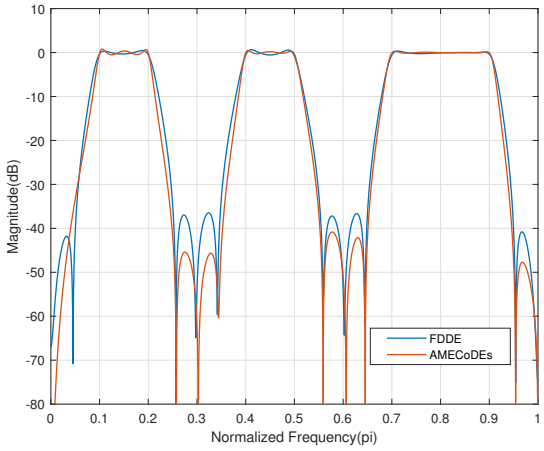


Fig. 8. Magnitude response of the asymmetrical triple-passband filter designed using FDDE and AMECoDEs algorithms.

$\epsilon$, $\mu^0_{F,M1}$, $\mu^0_{CR,M1}$, $\mu^0_{F,M2}$, and $\mu^0_{CR,M2}$ correspond to the original AMECoDEs algorithm described in [39].

There are some differences between the AMECoDEs 1 and AMECoDEs 2 approaches. In AMECoDEs 1, the weight function follows a piecewise discrete linear form, whereas in AMECoDEs 2, it remains constant within each band. The filter structure also differs between the two methods: AMECoDEs 1 employs randomly connected subsystems in cascade or parallel, with the configuration evolving throughout the optimization process, whereas AMECoDEs 2 maintains a fixed structure consisting of a serial connection of second-order sections. Additionally, in AMECoDEs 1, each second-order section (SOS) utilizes a first-order numerator biquad, requiring some zeros of the transfer function to be located at the origin. In contrast, AMECoDEs 2 employs a full biquad with a second-degree numerator polynomial, offering greater flexibility in zero placement during evolution. Another key distinction lies in the computation of the mean squared error: AMECoDEs 1 uses 128 sampling points, while AMECoDEs 2 employs 101.

TABLE VI. CHARACTERISTICS OF CLASSICAL FILTERS DESIGNED USING AMECODES 1, AMECODES 2, AND FDDE APPROACHES

| Filter type | Characteristic | AMECoDEs 1 [a] | AMECoDEs 2 | FDDE |
|---|---|---|---|---|
| Low-pass | $\delta_{pass1}$ | 0.1244 | 0.1268 | 0.1264 |
| | $\delta_{pass2}$ | - | - | - |
| | $A_{stop1}$ (dB) | 55.3502 | 60.2884 | 60.2647 |
| | $A_{stop2}$ (dB) | - | - | - |
| | $\Delta\omega_1$ ($\pi$) | 0.0611 | 0.0496 | 0.0496 |
| | $\Delta\omega_2$ ($\pi$) | - | - | - |
| High-pass | $\delta_{pass1}$ | 0.1238 | 0.0891 | 0.0885 |
| | $\delta_{pass2}$ | - | - | - |
| | $A_{stop1}$ (dB) | 56.5713 | 62.3108 | 62.3158 |
| | $A_{stop2}$ (dB) | - | - | - |
| | $\Delta\omega_1$ ($\pi$) | 0.0545 | 0.0491 | 0.0491 |
| | $\Delta\omega_2$ ($\pi$) | - | - | - |
| Band-pass | $\delta_{pass1}$ | 0.0527 | 0.0945 | 0.086 |
| | $\delta_{pass2}$ | - | - | - |
| | $A_{stop1}$ (dB) | 28.9837 | 34.7622 | 35.6075 |
| | $A_{stop2}$ (dB) | 28.9805 | 34.7688 | 35.6075 |
| | $\Delta\omega_1$ ($\pi$) | 0.0559 | 0.0588 | 0.0573 |
| | $\Delta\omega_2$ ($\pi$) | 0.0558 | 0.0588 | 0.0573 |
| Band-stop | $\delta_{pass1}$ | 0.0942 | 0.0931 | 0.093 |
| | $\delta_{pass2}$ | 0.1097 | 0.093 | 0.093 |
| | $A_{stop1}$ (dB) | 29.2054 | 35.3809 | 35.3766 |
| | $A_{stop2}$ (dB) | - | - | - |
| | $\Delta\omega_1$ ($\pi$) | 0.0615 | 0.0544 | 0.0544 |
| | $\Delta\omega_2$ ($\pi$) | 0.0615 | 0.0544 | 0.0544 |

[a] The values have been taken from [19].

TABLE VII. CHARACTERISTICS OF DUAL-PASSBAND FILTERS DESIGNED USING AMECODES 1, AMECODES 2, AND FDDE APPROACHES

| Filter type | Characteristic | AMECoDEs 1 [a] | AMECoDEs 2 | FDDE |
|---|---|---|---|---|
| Symmetrical dual-passband | $A_{pass1}$ (dB) | 0.25 | 0.16 | 0.15 |
| | $A_{pass2}$ (dB) | 0.47 | 0.17 | 0.13 |
| | $A_{stop1}$ (dB) | 28 | 44 | 45 |
| | $A_{stop2}$ (dB) | 30 | 46 | 46 |
| | $A_{stop3}$ (dB) | 23 | 45 | 43 |
| Asymmetrical dual-passband | $A_{pass1}$ (dB) | 0.29 | 0.12 | 0.19 |
| | $A_{pass2}$ (dB) | 0.17 | 0.14 | 0.24 |
| | $A_{stop1}$ (dB) | 28 | 62 | 41 |
| | $A_{stop2}$ (dB) | 27 | 50 | 44 |
| | $A_{stop3}$ (dB) | 24 | 58 | 41 |

[a] The values have been taken from [20].

### C. Analysis of the Designed Triple-Passband IIR Filters

For the triple-bandpass filters, both symmetric and asymmetric, designed using the FDDE and AMECoDEs algorithms, the mean squared errors are compared in Table V. The magnitude responses of these filters are also compared in Fig. 7 and 8. The comparison results indicate that the AMECoDEs algorithm achieves a lower mean squared error, which is reflected in higher minimum attenuation levels in the stopbands.

For the asymmetric triple-bandpass filter designed using the AMECoDEs algorithm, the maximum attenuations in the passbands and the minimum attenuations in the stopbands were determined, yielding the following values: the maximum attenuations in the three passbands, from left to right, are 1.3,

TABLE VIII. PARAMETERS OF THE AMECODES 1, AMECODES 2, AND FDDE APPROACHES

| Parameter | Approach | | |
|---|---|---|---|
| | ***AMECoDEs 1*** | ***AMECoDEs 2*** | ***FDDE*** |
| Population size (NP) | 100 | 100 | 100 |
| Maximum number of generations (MNG) (in thousands): (classic, dual-passband, triple-passband) | (100, 10, -) | (40, 40, 80) | (40, 40, 80) |
| Weight function | Linear | Constant | Constant |
| Filter structure | Optimal | Serial | Serial |
| Number of SOS for filter (D): (classic, dual-passband, triple-passband) | (4, 7, -) | (4, 7, 10) | (4, 7, 10) |
| Number of sampling points (N) | 128 | 101 | 101 |
| Numerator polynomial degree in SOS | 1 | 2 | 2 |
| Constant factor in mutation operation (CF) | - | - | 0.5 |
| Constant factor probability (CFP) | - | - | 0.7 |
| Scale factor (F) | Cauchy generator | Cauchy generator | - |
| Crossover rate (CR) | Gaussian generator | Gaussian generator | 0.5 |
| $p$ | 0.1 | 0.1 | - |
| $c$ | 0.1 | 0.1 | - |
| $\epsilon$ | 0.001 | 0.001 | - |
| $\mu^0_{F,M1}$ | 0.5 | 0.5 | - |
| $\mu^0_{CR,M1}$ | 0.5 | 0.5 | - |
| $\mu^0_{F,M2}$ | 0.5 | 0.5 | - |
| $\mu^0_{CR,M2}$ | 0.5 | 0.5 | - |

TABLE IX. COMPARISON OF CONTRIBUTIONS WITH RECENT RELATED WORKS

| Contribution | Chen et al. [19] | Chen et al. [20] | This Work |
|---|---|---|---|
| AMECoDEs algorithm applied to IIR filter design | Yes | Yes | Yes |
| FDDE algorithm applied to IIR filter design | No | No | Yes |
| Classical IIR filters design | Yes | No | Yes |
| Dual-passband IIR filters design | No | Yes | Yes |
| Triple-passband IIR filters design | No | No | Yes |
| Implementation validation on a development board | No | No | Yes |

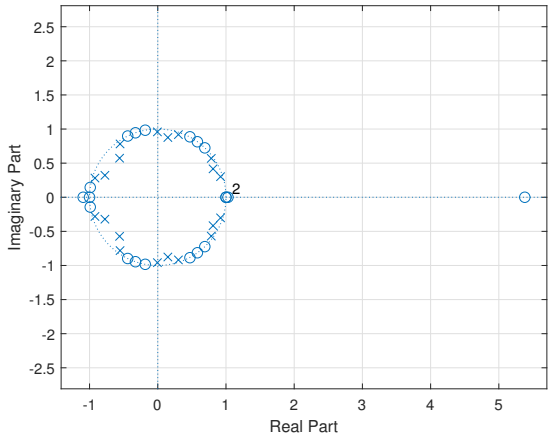


Fig. 9. Pole-zero diagram of the asymmetrical triple-passband filter designed using the AMECoDEs algorithm.

0.8, and 0.4 dB, while the minimum attenuations in the four stopbands, in the same order, are 33, 45, 41, and 48 dB. For this filter, the pole-zero diagram of the filter's transfer function is presented in Fig. 9, where its stability is verified, as all poles are located within the unit circle. Additionally, Table X provides the coefficients of the second-order sections of the filter: $b_0$, $b_1$, and $b_2$ correspond to the numerator coefficients, whereas $a_0$, $a_1$, and $a_2$ represent the denominator coefficients for each second-order section.

To evaluate the filter's performance, it was implemented on the OMAP-L138 LCDK development board using a serial structure of second-order sections, each in the transposed direct form II, with a sampling frequency of 16 kHz. A white noise signal was applied to the filter's input, whose spectrum is shown in Fig. 10a, and the spectrum of the filter's output signal was obtained, as depicted in Fig. 10b. Considering that the white noise signal has a finite duration and its spectrum is not perfectly flat, it can be concluded that the output signal spectrum closely approximates the filter's magnitude response shown in Fig. 8, thereby validating the proper operation of the triple-bandpass filter. The spectra were obtained using the Audacity software.

Table IX presents a summary of the comparison between the contributions of this work and those of recent related studies.

### D. Limitations of the Proposed Study

One of the primary limitations of this study is that the filter order must be predetermined before applying the AMECoDEs or FDDE algorithms. For instance, in our work, the filter order was set to 8 for classical IIR filters (4 SOS) and 14 for dual-passband IIR filters (7 SOS), consistent with the previous studies used for comparison. While this approach ensures a fair and direct performance comparison, it restricts the flexibility of the optimization process. Ideally, the filter order could be treated as an additional parameter to be optimized within the evolutionary process itself.

Another limitation concerns the selection of constant weight function for the mean squared error calculation. In our study, we assigned values as follows: $C_{\text{pass}} = 1$ (passband weight), $C_{\text{tran}} = 0$ (transition band weight), and $C_{\text{stop}}$ (stopband weight). The value of $C_{\text{stop}}$ was empirically adjusted, as described earlier. While this method provided satisfactory results, an optimal selection of $C_{\text{stop}}$ could enhance the overall performance of the filter design. A more effective approach would be to incorporate the determination of $C_{\text{stop}}$ within the evolutionary optimization process itself, allowing the algorithm to adaptively select the most suitable weight.

## VIII. CONCLUSION

In this study, infinite impulse response (IIR) digital filters were designed using the differential evolution algorithms

TABLE X. SECOND-ORDER SECTION COEFFICIENTS OF ASYMMETRICAL TRIPLE-PASSBAND IIR FILTER DESIGNED USING THE AMECODES ALGORITHM

| $b_0$ | $b_1$ | $b_2$ | $a_0$ | $a_1$ | $a_2$ |
|---|---|---|---|---|---|
| 7.8876236290 | 5.1604815420 | 7.8872954230 | 1 | -0.2960674528 | 0.7889534529 |
| -2.176918181E+06 | -1.392950347E+05 | 2.448781388E+06 | 1 | -1.6210903460 | 0.8305176942 |
| -3.7806622860 | 3.5658678580 | -3.8096999700 | 1 | -1.5689265950 | 0.9398252056 |
| 1.3770756250 | -8.7861671130 | 7.4077929170 | 1 | -1.8412102950 | 0.9386775773 |
| 0.0004063950 | 0.0001492708 | 0.0004064004 | 1 | 0.0104678515 | 0.9183642167 |
| 0.7727905120 | 0.6808875185 | 0.7728040981 | 1 | 1.1192169280 | 0.6412596450 |
| 2.0805008130 | 0.0002940766 | -2.0811039430 | 1 | 1.8416581300 | 0.9272396429 |
| -0.9361654924 | -1.8536317010 | -0.9369053235 | 1 | 1.1053408530 | 0.9166266723 |
| -0.0636657429 | 0.0878348434 | -0.0636581859 | 1 | -0.6053174239 | 0.9350729683 |
| -0.0000042933 | 0.0000049894 | -0.0000042919 | 1 | 1.5495830260 | 0.7037222684 |

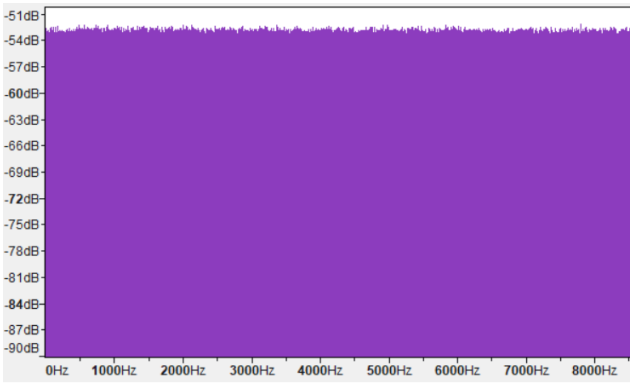


(a) Spectrum of the white noise input signal.

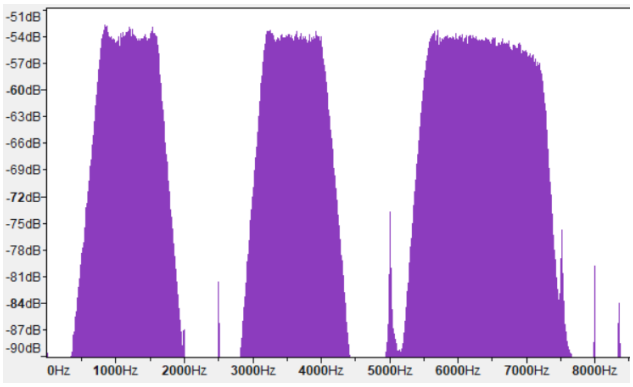


(b) Output signal spectrum of the asymmetric triple-passband IIR filter implemented on the OMAP-L138 LCDK board.

Fig. 10. Spectrum comparison before and after filtering with the OMAP-L138 LCDK.

AMECoDEs and FDDE. The designed filters encompass both classical filters—low-pass, high-pass, band-pass, and band-stop filters—as well as multi-passband filters, including symmetric dual-passband, asymmetric dual-passband, symmetric triple-passband, and asymmetric triple-passband filters. A structure based on a serial connection of second-order sections was adopted for their implementation. The fitness evaluation criterion was the mean squared error (MSE), computed using a constant weight function within each frequency band.

The theoretical contribution of this study is the adaptation of the FDDE algorithm, initially proposed in a general framework by Jianchao Cheng et al. in [40], to the design of IIR digital filters, expanding its applicability within digital signal processing. Additionally, the comparative analysis between FDDE and AMECoDEs algorithms offers new insights into their respective advantages and trade-offs, particularly in designing classical and multi-passband filters. On the practical side, the developed filters are applicable to various signal processing tasks, including audio processing, biomedical signal analysis, communication systems, and industrial control, demonstrating the real-world utility of the proposed approach.

This study presents four key contributions at the intersection of evolutionary algorithms and digital signal processing: (1) the novel adaptation of the FDDE algorithm for IIR digital filter design, expanding its applicability to signal processing applications; (2) a comparative analysis of the FDDE and AMECoDEs algorithms for classical and multi-passband IIR filters, highlighting their respective advantages in optimization performance; (3) the use of a fitness evaluation based on the mean squared error, calculated with a constant weight function within frequency bands, in contrast to previous methodologies that employed a linear weight function; and (4) the first implementation of differential evolution algorithms for triple-passband IIR filter design, validated through successful experimental implementation on a hardware development board.

The practical advantage of this study lies in the enhanced performance of the designed IIR filters, particularly in terms of stopband attenuation. The results indicate that the AMECoDEs-2 and FDDE approaches consistently achieve greater stopband attenuation—approximately 5 dB for classical filters and 13 dB for dual-passband filters—compared to previous works.

A key limitation of this study is the need to predefine the filter order before applying the AMECoDEs or FDDE algorithms. In this work, the filter order was set to 8 for classical IIR filters and 14 for dual-passband IIR filters, consistent with previous studies used for comparison. Another limitation concerns the selection of a constant weight function for the mean squared error (MSE) calculation. In this study, the passband and transition band weights were fixed at 1 and 0, respectively, while the stopband weight was empirically adjusted.

Future research should focus on enhancing the adaptability of the evolutionary optimization process in IIR filter design. One key direction is the integration of filter order as an optimization parameter rather than a predefined value. Addi-

tionally, refining the selection of weight factors in the mean squared error calculation is essential. Rather than relying on empirical adjustments for the stopband weight $C_{\text{stop}}$, future studies should implement an adaptive optimization strategy that allows the algorithm to automatically determine these values. Furthermore, an important avenue for future research is the evaluation of the algorithm proposed by Luo et al. [41] for IIR digital filter optimization, as its application could further improve design efficiency and overall filter performance.

## REFERENCES

[1] S. J. Schlecht, L. Fierro, V. Valimaki, and J. Backman, "Audio peak reduction using a synced allpass filter," in *2022 IEEE International Conference on Acoustics, Speech and Signal Processing (ICASSP)*, ser. International Conference on Acoustics Speech and Signal Processing ICASSP. Inst Elect & Elect Engineers; Inst Elect & Elect Engineers Signal Proc Soc, 2022, pp. 1006–1010, 47th IEEE International Conference on Acoustics, Speech and Signal Processing (ICASSP), Singapore, Singapore, May 22-27, 2022.

[2] V. Bruschi, S. Nobili, A. Terenzi, and S. Cecchi, "A low-complexity linear-phase graphic audio equalizer based on IFIR filters," *IEEE Signal Processing Letters*, vol. 28, pp. 429–433, 2021.

[3] S. Zhang and T. R. Gadekallu, "Digital interference signal filtering on laser interface for optical fiber communication," *EAI Endorsed Transactions on Scalable Information Systems*, vol. 10, no. 2, p. e14, Nov. 2022.

[4] S. Chen, Q. Zhao, Y. Ye, and B. Qu, "Using IIR filter in fractional order phase lead compensation PIMR-RC for grid-tied inverters," *IEEE Transactions on Industrial Electronics*, vol. 70, no. 9, pp. 9399–9409, SEP 2023.

[5] W.-W. Huang, L. Li, Z. Zhu, C. Hu, and L.-M. Zhu, "Notch-filter-based repetitive control of fast tool servos for high-performance tracking of periodic trajectories," *Precision Engineering*, vol. 88, pp. 125–134, 2024.

[6] R. Priyadharsini and A. Kunthavai, "Implementation of digital filters for real-time PPG signal processing in VLC," *Fluctuation and Noise Letters*, vol. 22, no. 01, p. 2350001, Feb 2023.

[7] L. M. Kannan and D. Deepa, "Low power very large scale integration (VLSI) design of finite impulse response (FIR) filter for biomedical imaging application." *DYNA*, vol. 96, no. 5, pp. 505–511, Sep-Oct 2021.

[8] M. Wisniewski and M. Wcislik, "Digital equalizer for data acquisition path, constructed using IIR filters," *IFAC Papersonline*, vol. 49, no. 25, pp. 342–345, 2016, 14th IFAC Conference on Programmable Devices and Embedded Systems (PDES), Brno, Czech Republic, Oct 05-07, 2016.

[9] O. Yakut, S. Solak, and E. D. Bolat, "IIR based digital filter design for denoising the ECG signal," *Journal of Polytechnic-Politeknik Dergisi*, vol. 21, no. 1, pp. 173–181, MAR 2018.

[10] R. Mohanraj and R. Vimala, "ECG signal denoising with field-programmable gate array implementation of fast digital finite impulse response and infinite impulse response filters," *Journal of Medical Imaging and Health Informatics*, vol. 10, no. 1, pp. 81–85, JAN 2020.

[11] S. Saha and S. Barman Mandal, "FPGA implementation of IIR elliptic filters for de-noising ECG signal," *Biomedical Signal Processing and Control*, vol. 96, p. 106544, 2024.

[12] M. Kowalczyk and T. Kryjak, "Hardware architecture for high throughput event visual data filtering with matrix of IIR filters algorithm," in *2022 25th Euromicro Conference on Digital System Design (DSD)*, ser. Euromicro Conference Proceedings, H. Fabelo, S. Ortega, and A. Skavhaug, Eds., 2022, pp. 284–291, 25th Euromicro Conference on Digital System Design (DSD), Maspalomas, Spain, Aug 31-Sep 02, 2022.

[13] V. Pathak, S. J. Nanda, A. M. Joshi, and S. S. Sahu, "Identification of characteristics frequency and hot-spots in protein sequence of COVID-19 disease," *Biomedical Signal Processing and Control*, vol. 78, p. 103909, 2022.

[14] N. Agrawal, A. Kumar, V. Bajaj, and G. Singh, "Design of digital IIR filter: A research survey," *Applied Acoustics*, vol. 172, p. 107669, 2021.

[15] N. Agrawal, A. Kumar, and V. Bajaj, "Design of infinite impulse response filter using fractional derivative constraints and hybrid particle swarm optimization," *Circuits Systems and Signal Processing*, vol. 39, no. 12, pp. 6162–6190, DEC 2020.

[16] S. Chauhan, M. Singh, and A. K. Aggarwal, "Designing of optimal digital IIR filter in the multi-objective framework using an evolutionary algorithm," *Engineering Applications of Artificial Intelligence*, vol. 119, p. 105803, 2023.

[17] Y. Wu, "Optimizing IIR filter design using multi-objective genetic algorithm: A focus on passband ripple and stopband attenuation," 2024, Conference paper, p. 64 – 69.

[18] P. Stubberud, "Digital IIR filter design using a differential evolution algorithm with polar coordinates," in *2022 IEEE 12th Annual Computing and Communication Workshop and Conference (CCWC)*. IEEE; IEEE USA; IEEE Reg 1; SMART; Inst Engn & Management; Univ Engn & Management, 2022, pp. 1029–1035, iEEE 12th Annual Computing and Communication Workshop and Conference (CCWC), Electr Network, JAN 26-29, 2022.

[19] L. Chen, M. Liu, Z. Wang, and Z. Dai, "A structure evolution-based design for stable IIR digital filters using AMECoDEs algorithm," *Soft Computing*, vol. 24, no. 7, pp. 5151–5163, Apr 2020.

[20] L. Chen, J. Wang, M. Liu, and C.-H. Chen, "A novel design method for dual-passband IIR digital filters," *Applied Intelligence*, vol. 50, no. 7, pp. 2132–2150, Jul 2020.

[21] M. Nakamoto and N. Aikawa, "Minimax design of sparse IIR filters using sparse linear programming," *IEICE Transactions on Fundamentals of Electronics Communications and Computer Sciences*, vol. E104A, no. 8, pp. 1006–1018, AUG 2021.

[22] S. R. Kalidindi, S. K. Terlapu, and M. V. Krishna, "Implementation of area efficient multiple passband FIR filter for 5G applications," *Journal of Scientific and Industrial Research*, vol. 80, no. 11, p. 971 – 978, 2021.

[23] V. Patel and A. Shah, "Denoising electrocardiogram signals using multiband filter and its implementation on FPGA," *Serbian Journal of Electrical Engineering*, vol. 19, no. 2, p. 115 – 128, 2022.

[24] P. Zahradnik, M. Vlcek, and B. Simak, "Equiripple FIR triple narrow band filters," in *APCCAS 2002: Asia-Pacific Conference on Circuits and Systems, VOL 1, Proceedings*. IEEE; CAS; ITB, Dept Electr Engn; ITS; IURC ME; JICA, 2002, pp. 83–86, asia-Pacific Conference on Circuits and Systems, Bali, Indonesia, Oct 28-31, 2002.

[25] F. Xiao, "Fast design of IIR digital filters with a general chebyshev characteristic," *IEEE Transactions on Circuits and Systems II-Express Briefs*, vol. 61, no. 12, pp. 962–966, DEC 2014.

[26] A. B. Bogatyrev, S. A. Goreinov, and S. Y. Lyamaev, "Efficient synthesis of optimal multiband filter," *Russian Journal of Numerical Analysis and Mathematical Modelling*, vol. 32, no. 4, pp. 217–223, AUG 2017.

[27] R. Wu, X. Tang, J. He, Y. Cao, L. Xiao, and F. Xiao, "The DST-O method for multiband IIR filter," *Circuits Systems and Signal Processing*, vol. 42, no. 1, pp. 431–448, JAN 2023.

[28] R. Storn and K. Price, "Differential evolution - a simple and efficient heuristic for global optimization over continuous spaces," *Journal of Global Optimization*, vol. 11, pp. 341–359, 01 1997.

[29] M. F. Ahmad, N. A. M. Isa, W. H. Lim, and K. M. Ang, "Differential evolution: A recent review based on state-of-the-art works," *Alexandria Engineering Journal*, vol. 61, no. 5, pp. 3831–3872, May 2022.

[30] Y. Xue, Y. Tong, and F. Neri, "An ensemble of differential evolution and adam for training feed-forward neural networks," *Information Sciences*, vol. 608, pp. 453–471, AUG 2022.

[31] T. Hielscher and S. Hadigheh, "Optimizing memory-efficient multi-modal networks for image classification using differential evolution," *Applied Soft Computing*, vol. 171, p. 112714, 2025.

[32] Y. Wang, S. Chen, and P. Zhang, "Position-posture control strategy for planar underactuated manipulators with second-order nonholonomic constraint," *International Journal of Control Automation and Systems*, vol. 20, no. 12, pp. 4015–4025, DEC 2022.

[33] S. Gupta, A. Kumar, V. Kumar, S. Singh, Sachin, and M. Gautam, "Autonomous underwater vehicle path planning using fitness-based differential evolution algorithm," *Journal of Computational Science*, vol. 85, p. 102498, 2025.

[34] X. Chen, W. Feng, S. You, Y. Hu, Y. Wan, and B. Zhao, "Dual temperature parameter control of pemfc stack based on improved differential evolution algorithm," *Renewable Energy*, vol. 241, p. 122319, 2025.

[35] K. Kashyap, S. Pathak, and N. S. Yadav, "Optimization of spreading code using modified differential evolution for wireless communication," *Wireless Personal Communications*, vol. 122, no. 2, pp. 1283–1304, JAN 2022.

[36] P.-Q. Huang, Y. Zhou, K. Wang, and B.-C. Wang, "Placement optimization for multi-IRS-aided wireless communications: An adaptive differential evolution algorithm," *IEEE Wireless Communications Letters*, vol. 11, no. 5, pp. 942–946, May 2022.

[37] Z. Cao, H. Jia, Z. Wang, C. H. Foh, and F. Tian, "A differential evolution with autonomous strategy selection and its application in remote sensing image denoising," *Expert Systems with Applications*, vol. 238, p. 122108, 2024.

[38] S. Das, S. S. Mullick, and P. Suganthan, "Recent advances in differential evolution – an updated survey," *Swarm and Evolutionary Computation*, vol. 27, pp. 1–30, 2016.

[39] L. Cui, G. Li, Z. Zhu, Q. Lin, K.-C. Wong, J. Chen, N. Lu, and J. Lu, "Adaptive multiple-elites-guided composite differential evolution algorithm with a shift mechanism," *Information Sciences*, vol. 422, pp. 122–143, JAN 2018.

[40] J. Cheng, Z. Pan, H. Liang, Z. Gao, and J. Gao, "Differential evolution algorithm with fitness and diversity ranking-based mutation operator," *Swarm and Evolutionary Computation*, vol. 61, p. 100816, 2021.

[41] Z. Luo, X. Qian, and W. Song, "Enhanced differential evolution with hierarchical selection mutation and distance-based selection strategy," *Engineering Applications of Artificial Intelligence*, vol. 144, p. 110124, 2025.

[42] D. Pelusi, R. Mascella, and L. Tallini, "A fuzzy gravitational search algorithm to design optimal IIR filters," *Energies*, vol. 11, no. 4, 2018, all Open Access, Gold Open Access.

[43] B. Durmuş, G. Yavuz, and D. Aydin, "Adaptive IIR filter design using self-adaptive search equation based artificial bee colony algorithm," *Turkish Journal of Electrical Engineering and Computer Sciences*, vol. 27, no. 6, p. 4797 – 4817, 2019, all Open Access, Bronze Open Access.

[44] A. Mohammadi, S. H. Zahiri, S. M. Razavi, and P. N. Suganthan, "Design and modeling of adaptive IIR filtering systems using a weighted sum - variable length particle swarm optimization," *Applied Soft Computing*, vol. 109, p. 107529, 2021.

[45] Z. Qiang, S. Jing, W. Weilian, Y. Ruping, and C. Cheng, "Design of fourth-order IIR digital filter based on FPGA," 2019, p. 161 – 166.

[46] Y. Lenaphet and P. Meemon, "The implementation of digital filter on FPGA for the spectral fusing gabor domain optical coherence microscopy," 2020, Conference paper.